IOPscience iopscience.iop.org

Home Search Collections Journals About Contact us My IOPscience

Electrical properties of ferroelectric $(SrBi_2Ta_2O_9)_{1-x}(Bi_3TiNbO_9)_x$ solid solution

This article has been downloaded from IOPscience. Please scroll down to see the full text article.

1997 J. Phys.: Condens. Matter 9 10225

(http://iopscience.iop.org/0953-8984/9/46/020)

View the table of contents for this issue, or go to the journal homepage for more

Download details:
IP Address: 171.66.16.209
The article was downloaded on 14/05/2010 at 11:07

Please note that terms and conditions apply.

J. Phys.: Condens. Matter **9** (1997) 10225–10235. Printed in the UK PII: S0953-8984(97)84031-3

Electrical properties of ferroelectric $(SrBi_2Ta_2O_9)_{1-x}(Bi_3TiNbO_9)_x$ solid solution

Yongfei Zhu†, Xubai Zhang, Peizhi Gu, P C Joshi and S B Desu

Department of Materials Science and Engineering, 213 Holden Hall, Virginia Tech, Blacksburg, VA 24061-0237, USA

Received 7 May 1997, in final form 30 July 1997

Abstract. $(SrBi_2Ta_2O_9)_{1-x}(Bi_3TiNbO_9)_x$ ($(SBT)_{1-x}(BTN)_x$) bulk ceramic was fabricated by the conventional solid state reaction. The samples were characterized in terms of the structural, dielectric, ac conductivity, and ferroelectric properties. The solid solution samples exhibited improved electrical properties compared to end members SBT and BTN. The Curie temperature of the solid solution was found to increase linearly with increasing BTN content. The solid solution samples exhibited lower conductivity than the end members SBT and BTN. The solid solution showed higher remanent polarization, but higher coercive field than SBT. The present results indicate that the $(SBT)_{1-x}(BTN)_x$ solid solution may be a useful SBT-based material for FRAM applications.

1. Introduction

The intense research devoted to ferroelectric thin films in recent years has been motivated by their potential application in non-volatile memory and other electrical, optical and pyroelectric devices [1–4]. $Pb(Zr_xTi_{1-x})O_3$ (PZT) has been a promising candidate for non-volatile memory applications, e.g., ferroelectric RAM devices (FRAM). However, there are still some problems existing in PZT materials for non-volatile memory device applications, such as fatigue, aging, retention, and imprint. Among them, fatigue, a decrease in switchable polarization with increasing number of polarization reversals, is an important reliability issue for FRAM devices which use a destructive readout operation (switching of polarization at each read/write operation). To improve the fatigue characteristics of PZT-based capacitors, the most successful technique is using oxide electrodes. Even though the fatigue rate of PZT-based thin films is significantly improved by using the above technique, the electrical conductivity of the oxide electrodes is not as high as that of metal electrodes typically used, such as Pt. The lower conductivity of the oxide electrodes can contribute to undesirable characteristics of ferroelectric non-volatile memories, such as a higher RC time constant of the capacitor. In addition, oxide electrodes may lead to the formation of secondary non-ferroelectric phases during film growth if carefully controlled processing condition are not used [5, 6].

An alternative approach to control the fatigue problem in ferroelectric capacitors is to use other ferroelectric materials. Recently, capacitors based on layered perovskites such as $SrBi_2Ta_2O_9$ (SBT) and metallic electrodes such as Pt have generated interest because

† Author to whom correspondence should be addressed.

0953-8984/97/4610225+11$19.50 © 1997 IOP Publishing Ltd

of their negligible polarization fatigue ($>10^{12}$ cycles), long polarization retention, and very low leakage currents [7–11]. But the major limitations for the application of SBT are the high processing temperature ($\sim$700 °C) and lower remanent polarization (P_r) ($\sim$5–10 μC cm^{-2}), compared to the processing temperature of 600 °C and remanent polarization of 20–30 μC cm^{-2} for PZT. The high processing temperature of SBT makes it not easy to match the process of very-large-size-integrated circuit (VLSI) fabrication to produce high-quality non-volatile memory. One of the approaches to solve the problem is to solve the problems caused by the high processing temperature [12]. The other is to lower the SBT processing temperature.

It has been found that the microstructure of SBT thin film has a significant influence on the ferroelectric properties. The grain size of the polycrystal SBT thin film plays an important role in improving the SBT capacitor ferroelectric properties. Desu *et al* have noticed that minimum ferroelectric properties are exhibited only when the grains approach a critical size [13, 14]: the thin films show improved ferroelectric properties with increase of the grain size. Therefore it may be a good way to achieve a higher P_r and lower processing temperature by forming solid solutions of SBT and another ferroelectric material, which has higher P_r, larger grain size and lower processing temperature. Some SBT-based solid solutions, especially SBT/$SrBi_2Nb_2O_9$ (SBN) [9, 14], have been studied.

In this study, we added Bi_3TiNbO_9 (BTN) to $SrBi_2Ta_2O_9$ (SBT) to form a ferroelectric solid solution. Both BTN and SBT belong to the Aurivillus family of bismuth layered structure compounds of the general formula of (Bi_2O_2)–$(M_{n-1}R_nO_{3n+1})$ where M = Ba, Pb, Sr, Bi, K, or Na, n = 2, 3, 4, or 5 and R = Ti, Nb, or Ta. Both compounds have orthorhombic symmetry structure comprised of n perovskite-like units of nominal composition MRO_3 between Bi_2O_2 layers along the orthorhombic c-axis [15–18]. Bi in BTN occupies Bi and Sr sites in SBT, and Ti and Nb in BTN replace Ta in SBT. BTN has higher theoretically calculated saturation polarization (P_s) values of 27.7 μC cm^{-2}, compared to 14.4 μC cm^{-2} for SBT [23, 24].

In this paper, bulk $(SBT)_{1-x}(BTN)_x$ (x = 0, 0.2, 0.4, 0.6, 0.8, 1) samples were fabricated using conventional ceramic processing. The structural, dielectric, ac conductivity, and ferroelectric properties of the materials were determined and discussed. The results of the present study provided useful information to improve the properties of the $(SBT)_{1-x}(BTN)_x$ thin films.

2. Experimental details

Stoichiometric mixtures of $(SBT)_{1-x}(BTN)_x$ with x = 0, 0.2, 0.4, 0.6, 0.8, and 1.0 were prepared for the present study. $SrCo_3$ (Fisher Scientific), Ta_2O_5 (Fisher Scientific), TiO_2 (Alfa AESAR), and Nb_2O_5 (Fisher Scientific) were used as the starting materials for the preparation of bulk samples. The powders were mixed and ball milled in plastic jars using ethyl alcohol as dispersing media, and then dried. The powder mixture was then calcined at 1120 °C in a covered alumina crucible for 3 h. The calcined powder was pressed at 15 MPa to form pellets with diameter of 18.5 mm and then sintered at 1230 °C for 3 h. The BTN (x = 1.0) sample was sintered at a lower temperature of 1190 °C as it evaporated at higher temperatures.

The dielectric and impedance measurements were conducted on pellets with a typical thickness of 0.15 cm and an area of 2.0 cm^2. Platinum electrodes were attached to both the surfaces of the pellets using platinum paste. For ferroelectric measurements, the pellets with typical thickness of 0.04 cm were used. The Pt electrodes were deposited on both the surfaces by sputtering using a shadow mask with an area of 0.02 cm^2.

The complex impedance measurements were conducted using an HP4192A impedance analyser with a four-terminal configuration. The impedance measurements were conducted at different temperatures as a function of frequency in the range 50 Hz–1 MHz by applying a small ac signal of 50 mV amplitude. The measurement temperature was varied in the range 25–900 °C using a stand-alone oven controlled by an Omega-CN90000 temperature controller. The dielectric measurements were also conducted using an HP4192A impedance analyser. The ferroelectric properties were measured by using an RT66A ferroelectric test system with an external high-voltage (4 kV) supply (Trek-609D-6 high-voltage amplifier).

3. Results and discussion

3.1. Structure and morphology

Figure 1 shows the x-ray diffraction (XRD) patterns of the bulk samples with x in the range 0–10. The samples were found to be well crystallized in the orthorhombic single phase.

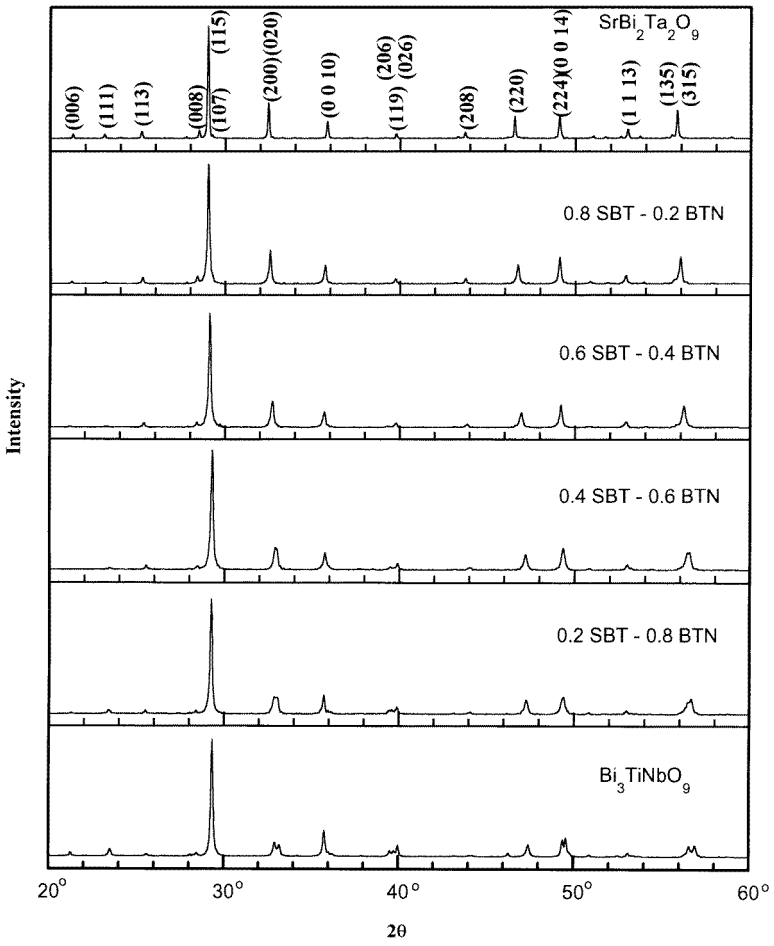

Figure 1. XRD patterns of $(SBT)_{1-x}(BTN)_x$ ($x = 0, 0.2, 0.4, 0.6, 0.8, 1$) samples. Powders were calcined at 1120 °C for 3 hours.

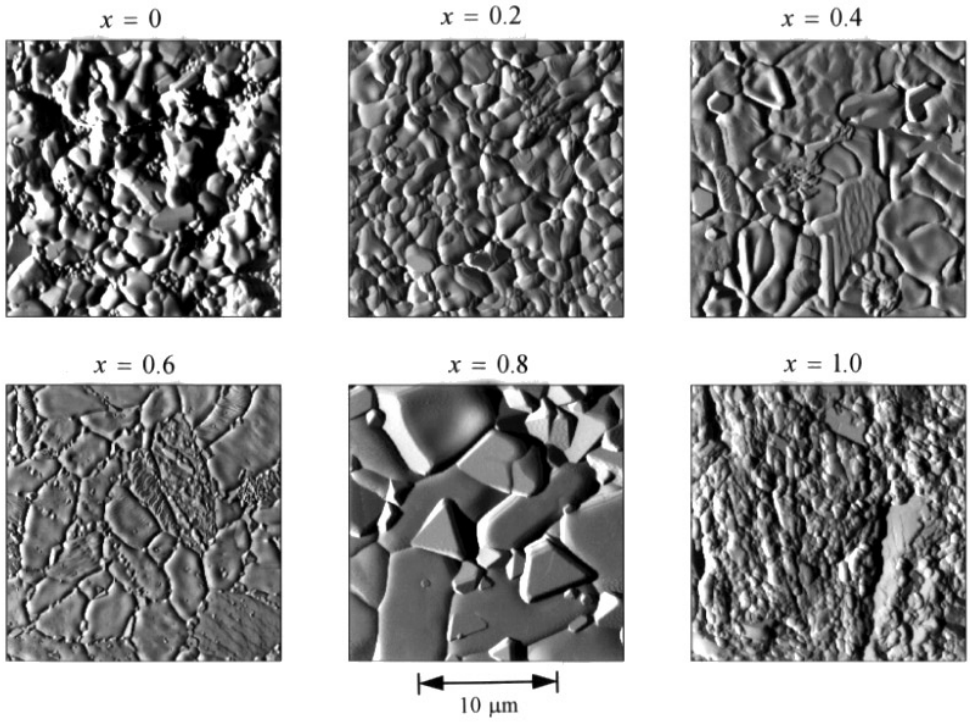

Figure 2. AFM pictures of $(SBT)_{1-x}(BTN)_x$ ($x = 0, 0.2, 0.4, 0.6, 0.8, 1$) samples. The bulk BTN sample was sintered at 1190 °C for 3 hours; the others were sintered at 1230 °C for 3 hours.

There were no detectable secondary phases, indicating the complete solid solution of the SBT and BTN compositions. It can be seen from figure 1 that all the patterns are similar, and the peaks [115], [020], [220], [224], [315], and [11$\underline{3}$] are shifting towards higher 2θ value with increase in the BTN content x. This slight shifting is caused by gradual distortion of the unit cell as the substitutional solid solution is formed. Figure 2 shows the atomic force micrographs (AFMs) of the solid solution compositions sintered under similar conditions and with x in the range 0–1.0. The grain size was found to increase with the increase in the BTN content x, and both pure SBT and BTN have the smallest grain size among the solid solutions.

3.2. Dielectric properties

The dielectric properties were measured in terms of the dielectric constant ε_r and loss factor $\tan\delta$. The dielectric measurements were conducted in the frequency range 10–1000 kHz as a function of temperature for the $(SBT)_{1-x}(BTN)_x$ system with $x = 0$, 0.2, 0.4, 0.6, and 0.8. It was not possible to measure the dielectric properties of BTN in the vicinity of its transition temperature because of its high conductivity.

Figure 3 shows the dielectric constant of the samples measured at 100 kHz as a function of temperature. The Curie temperature was found to increase with the increase in BTN content in the solid solution system. Figure 4 shows the Curie temperature as a function of BTN content x. The Curie temperature was found to increase linearly with the increase in the BTN content x. The Curie temperature of BTN was found to be 938 °C by extrapolation

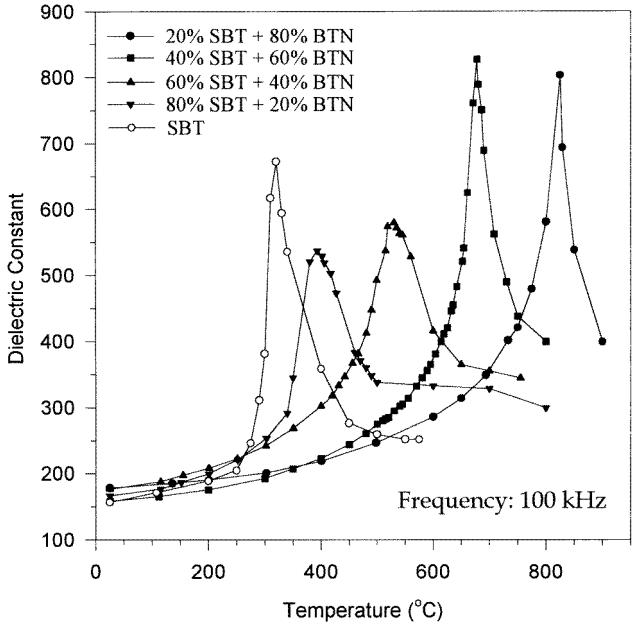

Figure 3. Temperature dependence of dielectric constant of $(SBT)_{1-x}(BTN)_x$ $(0 \leqslant x \leqslant 0.8)$ bulk solid solutions at the frequency of 100 kHz.

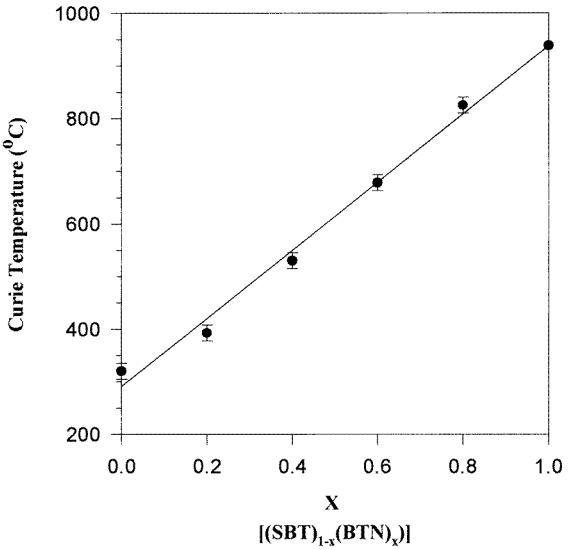

Figure 4. The relationship of Curie temperature and x in $(SBT)_{1-x}(BTN)_x$ solid solutions.

of the Curie temperature–x plot. The linearity of the Curie temperature suggests that a series of complete substitutional solid solutions was formed by mixing SBT and BTN. The formation of a complete substitutional solid solution is reasonable as SBT and BTN have the same layered-perovskite structure, the lattice parameter differences of SBT and BTN

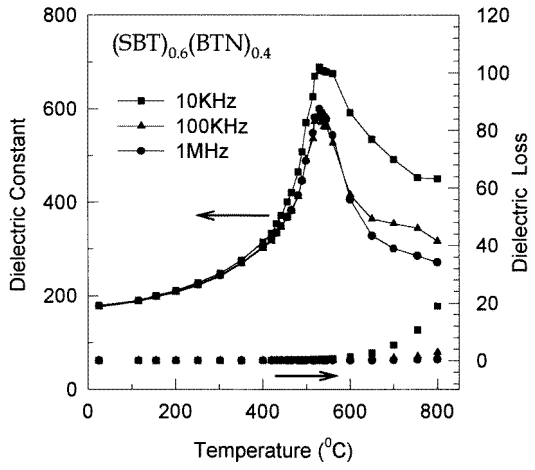

(a)

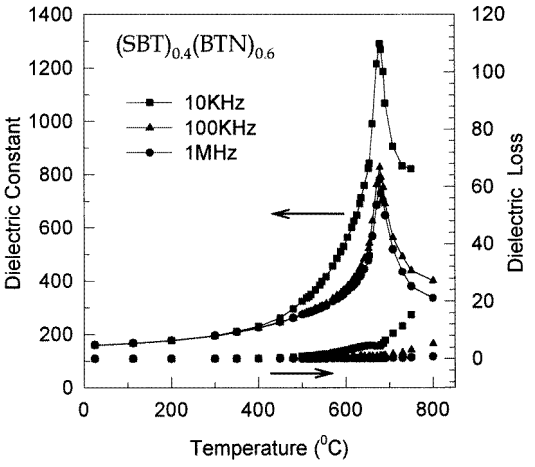

(b)

Figure 5. Temperature dependence of dielectric constant and loss ($\tan\delta$) at frequencies of 10, 100, and 1000 kHz for (a) $x = 0.4$ and (b) $x = 0.6$ $(SBT)_{1-x}(BTN)_x$ solid solutions.

are as low as 5%, and the differences of displacive ions are 2.65% for Sr^{2+} and Bi^{3+}, 5.7% for Ta^{5+}, Ti^{4+}, and Nb^{5+}.

It can also be seen from figure 3 that the samples with $x = 0$, 0.6, and 0.8 obey the Curie–Weiss law at temperature above the transition point while the samples with $x = 0.2$ and 0.4 exhibit broad dielectric constant peaks. The broad dielectric constant peak of the samples with $x = 0.2$ and 0.4 implies that the ferroelectric–paraelectric phase transition does not occur at discrete temperature but over a temperature range. The broad dielectric constant peak may be due to the variation of ferroelectric–paraelectric phase transitions from one unit cell to another, although these solid solutions show homogeneity in the macroscopic region. It appears that SBT and BTN are not resolved completely at atomic levels in the solid solutions with $x = 0.2$ and 0.4. Despite the existence of broad dielectric constant

peaks, we still selected the dielectric constant peak as the Curie temperature for samples with $x = 0.2$ and 0.4. The Curie–Weiss temperatures were found to be 189 °C, 606 °C, and 754 °C and the Curie constants were 8.2×10^4, 5.9×10^4, and 5.4×10^4 for samples with $x = 0$, 0.6, and 0.8, respectively, at an applied frequency of 100 kHz. The Curie–Weiss temperature of 189 °C for SBT is about the same as the reported value of 190 °C [19]; however, the Curie constant of 8.2×10^4 is lower than the published datum of 2.0×10^5 [19].

Figure 5 shows the typical dielectric constant and the loss factor–temperature plots measured at different frequencies for samples exhibiting sharp transition (e.g., sample with $x = 0.6$) and broad transition (e.g., sample with $x = 0.4$). The dielectric constant peaks were not found to shift with frequency in the range 10–1000 kHz for all the samples. The dielectric loss tangent was lower than 0.0008 for the entire solid solution system under room-temperature conditions and was found to increase in the vicinity of the Curie temperature. The dielectric constant peak found to be sharp for $x = 0.4$ and broad for $x = 0.4$ at all frequencies.

3.3. AC impedance and conductivity

The complex impedance of the samples was measured over a wide range of temperatures (25–900 °C) and frequencies (50 Hz–1 MHz). Each sample showed only one perfect semicircle arc (the high-frequency arc) in the low-temperature range (25–400 °C) with the semicircle centre slightly below the real axis. Figure 6 shows the typical complex impedance plot for a $(SBT)_{1-x}(BTN)_x$ sample measured at 25 °C and 485 °C. The semicircle radius was found to decrease with increasing temperature resulting in a smaller intercept on the real axis. The intercept on the real axis represents the sum of the resistances offered by intergrain and grain regions except electrode effects. In the higher temperature range (>400 °C), the semicircle was followed by an inclined straight line at lower frequencies, which may be due to electrode–ceramic interfacial effects. Similar effects have been observed in other materials by Armstrong *et al* [21] and Singh *et al* [22].

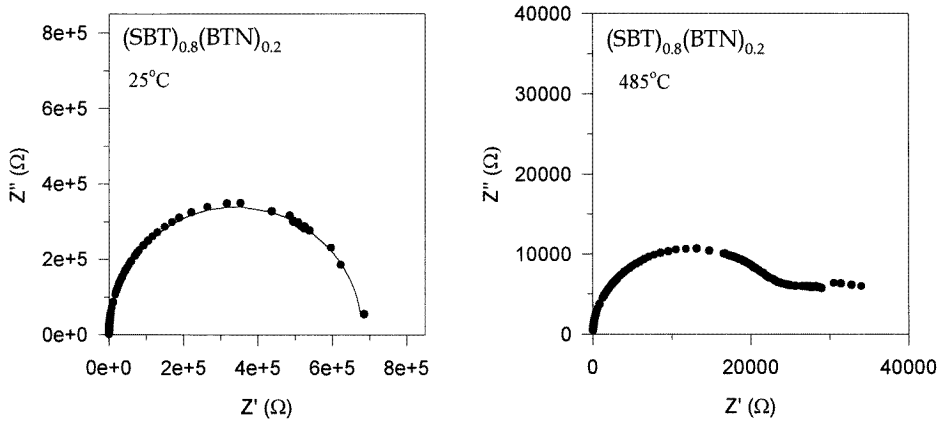

Figure 6. Complex impendance diagram for $(SBT)_{0.8}(BTN)_{0.2}$ at temperature of (a) 25 °C and (b) 485 °C.

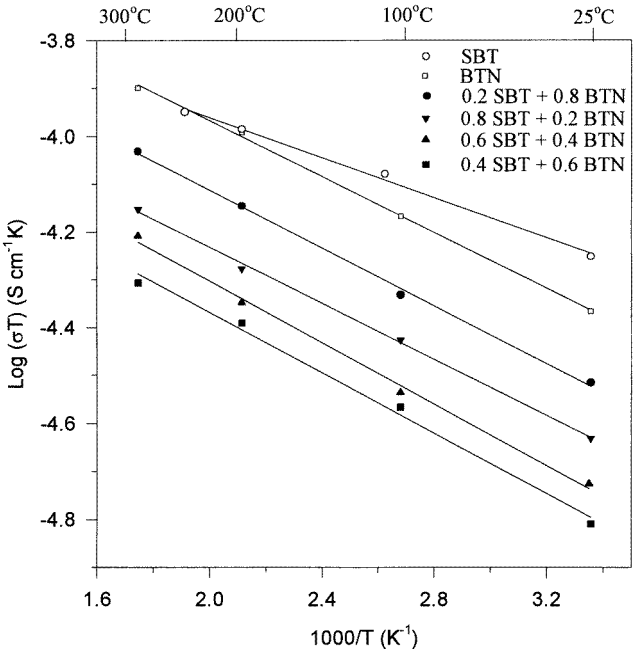

Figure 7. The variation of electrical conductivity as a function of temperature for the $(SBT)_{1-x}(BTN)_x$ system in the low temperature range.

Figure 7 shows the $\log(\sigma T)$–$10^3/T$ plots measured in the low-temperature region for samples with x in the range 0–1.0. The conductivity σ was calculated from the semicircle radius. For all the samples, the conductivity was found to increase with the increase in temperature. The conductivity of various samples was found to vary in a small range with temperature and composition. In the low temperature range (25–300 °C), the conductivity of various samples obeyed the Arrhenius equation $\sigma T = (\sigma T)_0 \exp(-E/kT)$, where E is the activation energy, k is the Boltzmann constant, and T is the absolute temperature. The activation energies of various samples were found to be very close to each other as shown in table 1. Figure 8 shows the dependence of the room-temperature conductivity on the BTN content x. The conductivity of the solid solution compositions was found to be lower than the end members SBT and BTN. The lowest conductivity was obtained for the composition with $x = 0.6$. In the higher temperature range (>400 °C), the conductivity was found to increase at a much faster rate with temperature than in the low temperature range as shown in figure 9. The slopes for all the samples were close except for the $(SBT)_{0.2}(BTN)_{0.8}$ composition which exhibited almost double activation energy compared to other samples as shown in table 1. The end members SBT and BTN exhibited higher conductivity than other compositions even in the higher temperature range.

3.4. Ferroelectric properties

The ferroelectric hysteresis loops were measured at room temperature. It was possible to obtain good hysteresis loops only for samples with $x = 0$ and 0.2 as shown in figure 10. The $(SBT)_{0.8}(BTN)_{0.2}$ composition exhibited higher remanent polarization (14.4 μC cm^{-2}) and coercive field (40 kV cm^{-1}) values compared to the values of 11.8 μC cm^{-2} and

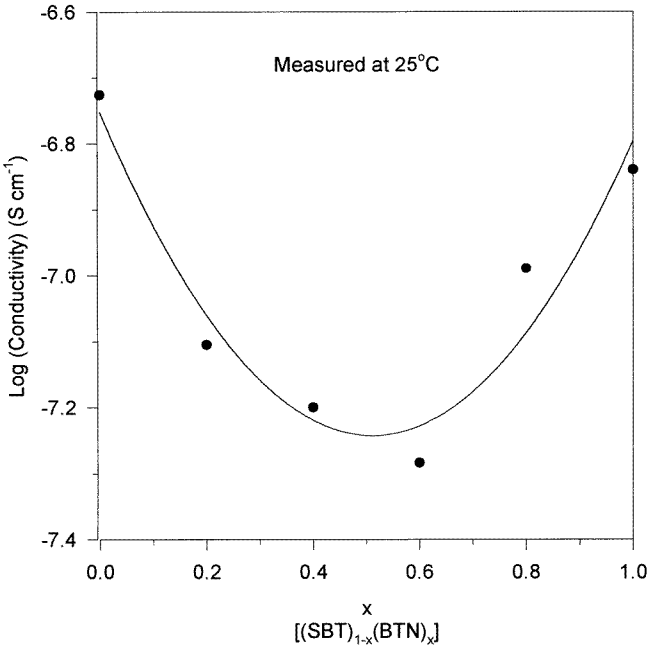

Figure 8. The relationship of conductivity and the solid solution composition in $(SBT)_{1-x}(BTN)_x$ at 25 °C.

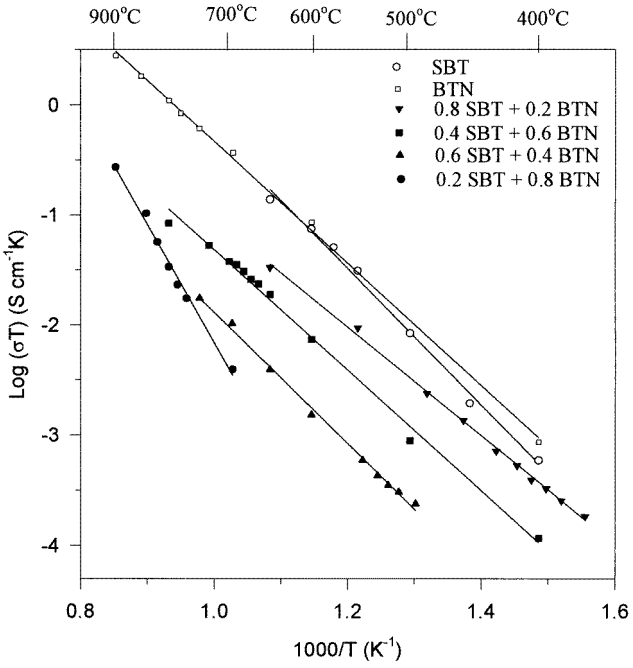

Figure 9. The variation of electrical conductivity as a function of temperature for the $(SBT)_{1-x}(BTN)_x$ system in the high temperature range.

Table 1. The activation energy (E) calculated from the Arrhenius equation.

	Activation energy (eV)	
x $((SBT)_{1-x}(BTN)_x)$	Low temperature (25–300 °C)	High temperature (400–900 °C)
0	0.018	0.524
0.2	0.025	0.425
0.4	0.028	0.512
0.6	0.027	0.471
0.8	0.026	0.929
1	0.025	0.478

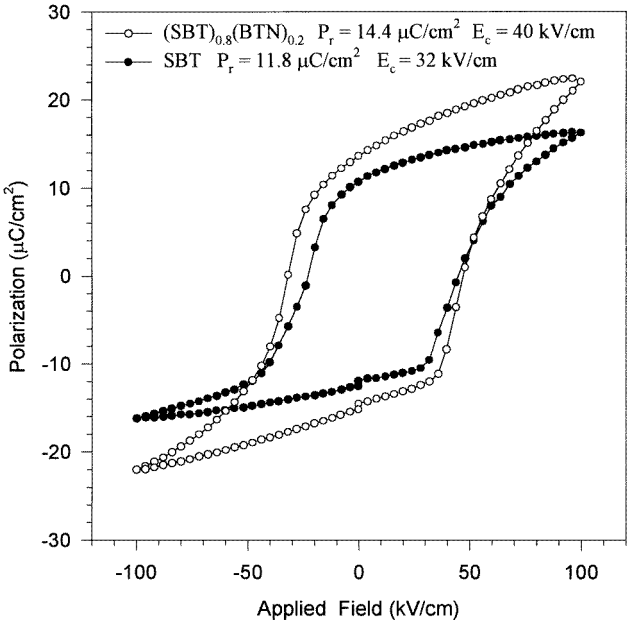

Figure 10. Hysteresis loops of the bulk SBT and $(SBT)_{0.8}(BTN)_{0.2}$ samples.

32 kV cm^{-1} for the SBT composition. The other samples did not show any hysteresis loop even at the maximum voltage of 4 kV ($\sim$100 kV cm^{-1}) applied by our external voltage source. This is possibly due to higher E_c of these samples causing the failure of domain direction alignment in these samples even at the maximum applied field possible with the present setup. It is difficult to make these brick samples thinner than 0.04 cm due to polishing and grinding problems at lower thickness.

4. Conclusions

$(SBT)_{1-x}(BTN)_x$ solid solution ceramics were fabricated by the conventional solid state reaction. The solid solution exhibited improved dielectric, conductivity, and ferroelectric properties compared to the SBT material. The important results are as follows.

(1) The $(SBT)_{0.8}(BTN)_{0.2}$ showed higher remanent polarization and coercive field compared to SBT material.

(2) The solid solution compositions exhibited lower conductivity than the end members SBT and BTN. The lowest conductivity was obtained for the composition with $x = 0.6$.

(3) The Curie temperature was found to increase linearly with increasing BTN content.

In addition to the fact that the solid solution has larger grain size than SBT [20], the solid solution shows improved electrical properties compared to SBT. The higher-Curie-temperature, lower-conductivity, and higher-remanent-polarization properties of the solid solution compared to SBT mean that it will probably become a useful SBT-based material for FRAM applications.

References

[1] Wu S Y 1974 *IEEE Trans. Electron Devices* **ED-21** 499
[2] Haertling G H 1990 *J. Vac. Sci. Technol.* **9** 414
[3] Francombe M H and Krishnaswamy S V 1990 *J. Vac. Sci. Technol.* A **8** 1382
[4] Scott J F and Paz de Araujo C A 1989 *Science* **246** 1400
[5] Dat R, Lee J K, Auciello O and Kingon A I 1995 *Appl. Phys. Lett.* **67** 572
[6] Auciello O, Al-Shareef H N, Gifford K D, Lichtenwalner D J, Dat R, Bellur K R, Kingon A I and Ramesh R 1994 *Mater. Res. Soc. Symp. Proc.* vol 341 (Pittsburgh, PA: Materials Research Society) p 341
[7] Desu S B and Vijay D P 1995 *Mater. Sci. Eng.* B **32** 75
[8] Paz de Araujo C A, Cuchlaro J D, McMillan L D, Scott M C and Scott J F 1995 *Nature* **374** 627
[9] Scott J F, Rose F M, Paz de Araujo C A, Scott M C and Huffman M 1996 *MRS Bull.* **21** 33
[10] Li T K, Zhu Y, Desu S B, Peng C and Nagata M 1996 *Appl. Phys. Lett.* **68** 29
[11] Desu S B and Li T K 1995 *Mater. Sci. Eng.* B **34** L4
[12] Katori K, Nagel N, Watanabe K, Tanaka M, Yamoto H and Yagi H 1997 *9th Int. Symp. on Integrated Ferroelectrics (Santa Fe, NM)*
[13] Nagata M, Vajay D P, Zhang X and Desu S B 1996 *Phys. Status Solidi* a **157** 75
[14] Chen T, Li T K, Zhang X and Desu S B 1997 *J. Mater. Res.* **12** 1569
[15] Aurivillus B 1949 *Ark. Kemi* **1** 463
[16] Subba Rao E C 1961 *J. Chem. Phys.* **34** 695
[17] Smolenskii G A, Isupov V A and Agranovskaya A I 1961 *Fiz. Tverd. Tela* **3** 895
[18] Newham R E, Wolfe R W, Horsey R S, Diaz-Colon F A and Kay M L 1973 *Mater. Res. Bull.* **8** 1183
[19] *Landolt–Börnstein New Series* 1981 vol 16, ed K-H Hellwege p 235
[20] Zhang Xubai, Gu Peizhi and Desu S B 1997 *Phys. Status Solidi* a **160** 35
[21] Armstrong R D, Dickinson T and Willis P M 1974 *J. Electroanal. Chem.* **53** 389
[22] Singh K, Chandrayan V R and Deshpande V K 1988 *Solid State Ion.* **28–30** 228
[23] Rae D A, Thomson J G and Withers R L 1992 *Acta Crystallogr.* B **48** 418
[24] Thompson J G, Rae A D, Withers R L and Craig D C 1991 *Acta Crystallogr.* B **47** 174